Multidimensional matter-wave beam splitters by multiphoton hyperfine Raman transitions

Xu-Dong Liu, Zong-You Chen, Wei-Chun Huang, Yang-Kao Lee, Yong-Fan Chen, and Pei-Chen Kuan[*]

Department of Physics, National Cheng Kung University, Tainan 70101, Taiwan

Multidimensional beamsplitters play crucial roles in the development of multidimensional atom interferometers and have the potential for applications in quantum information in higher dimensions. We present different configurations of multidimensional beamsplitters using both conventional two-photon Raman transitions and recently discovered four-photon Raman transitions. The differences between these configurations arise from the selection of external magnetic fields to serve as quantization axes. We explored and estimated statistical and systematic errors that may occur when multiple Raman transitions are used to construct multidimensional atom interferometers with deviated quantization axes. Our results demonstrated a tradeoff between the simplicity of axis alignment relative to the beams and the required optical power. These considerations are pertinent to the future design and optimization of multidimensional atom interferometry systems.

I. INTRODUCTION

Atom interferometry is an important tool for applications in precise measurement and quantum sensing [1–13]. It offers distinct advantages over photon-based methods in that it is sensitive to moving reference frames. Therefore, atom interferometers are suitable for use as inertial sensors for velocity, acceleration, and rotation detection [2,7,10,14–18]. Conventional inertial sensors measure acceleration and velocity separately through unidirectional apparatuses. However, to improve the efficiency and compactness of sensors, multidimensional atom interferometers have been proposed for use as inertial sensors [19]; such interferometers can execute multidimensional measurements of velocity, acceleration, and rotation simultaneously by using multidimensional beamsplitters. In addition to the applications in atom interferometry, operators based on multidimensional beamsplitters could also demonstrate quantum walk in the higher dimensions [20–22], exploring related potential in quantum simulation [22–24] and quantum algorithms [25–27].

Raman transitions involve the use of electromagnetic fields to create superpositions of different atomic states. They play a pivotal role in the coherent control of matter waves. In contrast to other types of atom-light interaction methods such as Bragg diffraction [28,29] and Bloch oscillations [30,31], Raman transitions are favored in the design of multidimensional atom interferometers for creating beamsplitters; this is because Raman transitions enable the use of different hyperfine ground states of atoms to facilitate signal detection in compact setups. However, the use of Raman transitions in multidimensional applications necessitates careful consideration of the direction of the external magnetic field. Improper alignment of the magnetic field can substantially suppress signals [32,33]. Here based on the recently reported four-photon Raman transitions [33], we realized multidimensional beamsplitters under
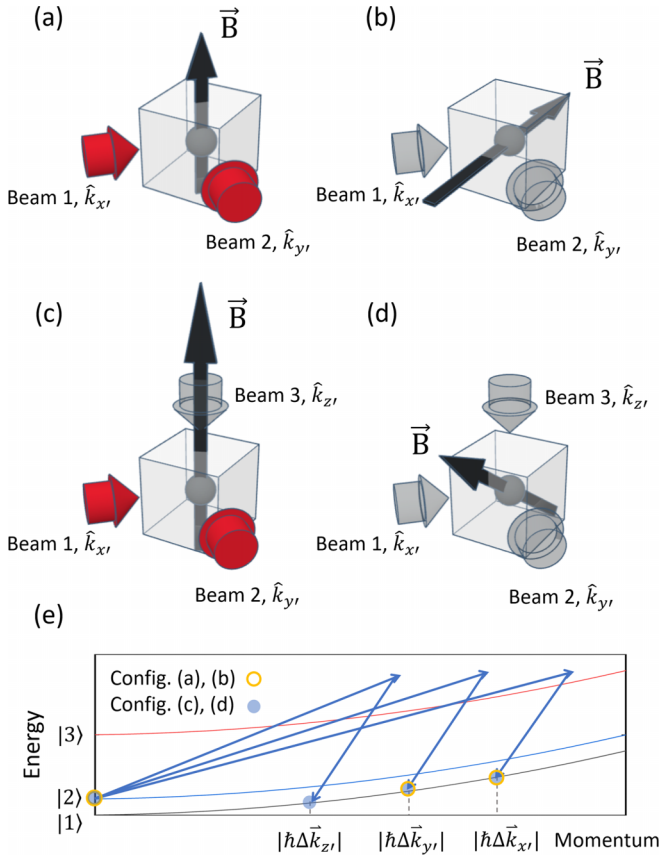
different configurations. In addition to regular two-photon Raman transitions, we also include four-photon Raman transitions as components of the multidimensional beamsplitters.

The different configurations are demonstrated in Figs. [1(a)–1(d)]. We attempted to develop both two-dimensional and three-dimensional copropagating beamsplitters by using two- and four-photon Raman transitions. Rather than one pair of beams driving atoms into moving in multiple orthogonal directions, here the difference in directions of atoms' velocities after the proposed beamsplitters comes from multiple pairs of beams [19]. A key distinction between two-photon and four-photon Raman transitions is that four-photon Raman transitions become predominant when the quantization axis is perpendicular, instead of being parallel, to the directions of the beams, which is typical for two-photon transitions. Therefore, by using combinations of the two Raman transitions, we could efficiently develop beamsplitters with different quantization axes. The related energy momentum is shown in Fig. 1(e). In the diagram, $\hbar$ is the reduced Planck's constant; $\Delta \vec{k}_{x'}$ represents the wave-vector difference in the Raman beams of $\hat{k}_{x'}$ direction. Similar definition holds for $\Delta \vec{k}_{y'}$ and $\Delta \vec{k}_{z'}$. Here due to the copropagating Raman beams, the four-photon Raman processes can be represented as two-photon Raman transitions with distinct dependence on power and magnetic fields of the effective Rabi frequency Ω_{eff} [33] and share similar representations as two-photon Raman transitions. In multidimensional beamsplitters, it is natural to require symmetry between directions. To cover different choices of the quantization axis, here we are considering two ways to symmetrically drive two-dimensional beamsplitters and two ways to symmetrically drive three-dimensional beamsplitters. We explored the advantages and disadvantages of the developed beamsplitters across various scenarios.
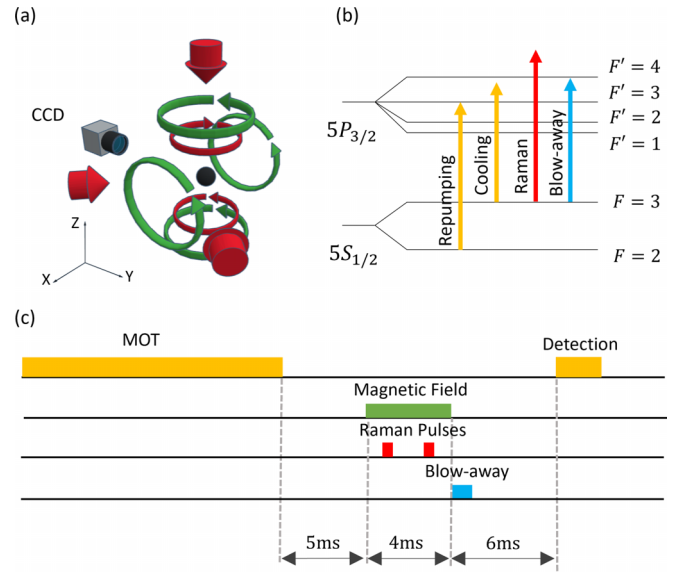
II. EXPERIMENTAL CONFIGURATION

We trapped and cooled ^{85}Rb atoms down to about 6 μK by using a standard magneto-optical trap (MOT) and polarization

―――――――――
*pckuan@phys.ncku.edu.tw

FIG. 1. Schemes for multidimensional beamsplitters. Black spots represent atoms in the vacuum chamber, with the external magnetic field $\vec{B}$ serving as the quantization axis. Solid arrows represent the four-photon Raman transitions, and hollow arrows represent the two-photon Raman transitions. The directions of the beams are orthogonal to each other and represented by $\hat{k}_{x'}$, $\hat{k}_{y'}$, and $\hat{k}_{z'}$, respectively. (a) Two-dimensional beamsplitter using two four-photon Raman transitions with the magnetic field oriented vertically. (b) Two-dimensional beamsplitter using two two-photon Raman transitions, with the direction of the magnetic field lying on the plane formed by the two beams and equidistant from them. (c) Three-dimensional beamsplitter combining two four-photon Raman transitions with one two-photon Raman transition, where the magnetic field is vertical. (d) Three-dimensional beamsplitter constructed from three two-photon Raman transitions, with the magnetic field centrally positioned among the three beams. (e) Energy-momentum diagram showing multidimensional beamsplitters associated with different configurations in (a)–(d). The scale has been exaggerated for clarity. Atoms are initially at rest. In the beamsplitters, atoms are in the superposition of different states, here demonstrated by circles in corresponding situations. The energy states $|1\rangle$ and $|2\rangle$ are ground states, and $|3\rangle$ demonstrates the excited state.

gradient cooling within a miniMOT vacuum system from coldQuanta. The laser system included two lasers and an amplifier. The laser for repumping was from a MOGLabs diode laser, whose frequency was stabilized to $|5S_{1/2}, F = 2\rangle \rightarrow |5P_{3/2}, F' = 3\rangle$. We seeded the cooling beam from another diode laser from MOGLabs to a tapered amplifier, BoosTA Pro from TOPTICA. The frequency was red-detuned by about 15 MHz relative to $|5S_{1/2}, F = 3\rangle \rightarrow |5P_{3/2}, F' = 4\rangle$.

FIG. 2. Experimental setup. (a) Configuration of the experiments. In addition to the anti-Helmholtz coils for the MOT, two external Helmholtz coils are used for generating uniform magnetic fields directing to $\hat{x}$ and $\hat{z}$ directions. (b) Level diagram of relevant atomic transitions for the experiment. (c) Demonstration of the time sequence of the experiment. The cooling repumping beams and MOT coils are switched off after the cold atomic ensemble is prepared during the MOT duration.

A diagram of the experimental apparatus is shown in Fig. 2(a). The relevant frequencies are demonstrated in Fig. 2(b).

After preparing the atoms, we shine circular-polarized Raman pulses to drive the Raman transition. The Raman laser beam passes through an iXblue fiber-coupled electro-optical modulator to generate the required frequency sidebands. The frequency differences between the carrier and the first sidebands are about the hyperfine splitting between two ground states of $|5S_{1/2}\rangle$ of ^{85}Rb. For defining the quantization axis, we apply two external magnetic fields through two Helmholtz coils. We assume one is in the $\hat{z}$ direction, and the other one is in the $\hat{x}$ direction. The magnitudes of the magnetic fields were regulated using voltage-controlled current sources that passed through the coils. The magnitudes of the magnetic fields were set to approximately 10 µT. There are overall three Raman beams here, directing to $(-\hat{x} + \hat{y})/\sqrt{2}$, $-(\hat{x} + \hat{y})/\sqrt{2}$, and $-\hat{z}$, respectively. These three directions are set to be $\hat{k}_{x'}$, $\hat{k}_{y'}$, and $\hat{k}_{z'}$, respectively. The beams are with $1/e^2$ beam waist of ≈ 3 mm and power of about 300 µW for the four-photon Raman transitions and of about 100 µW for the two-photon Raman transitions, respectively. By changing the quantization axis and beam intensity, we can change between the four configurations as demonstrated in Figs. [1(a)–1(d)].

We generate Ramsey fringes by shining two pulses to form two beamsplitters which are separated by 2 ms. Depending on the chosen configuration, the beamsplitters were operated in either two-dimensional [Figs. 1(a) and 1(b)] or three-dimensional modes [Figs. 1(c) and 1(d)]. After the pulses, some of the atoms are therefore transferred from $F = 3$ to 2 state. The atoms remaining in $F = 3$ are pushed away by a laser with the cycling transition
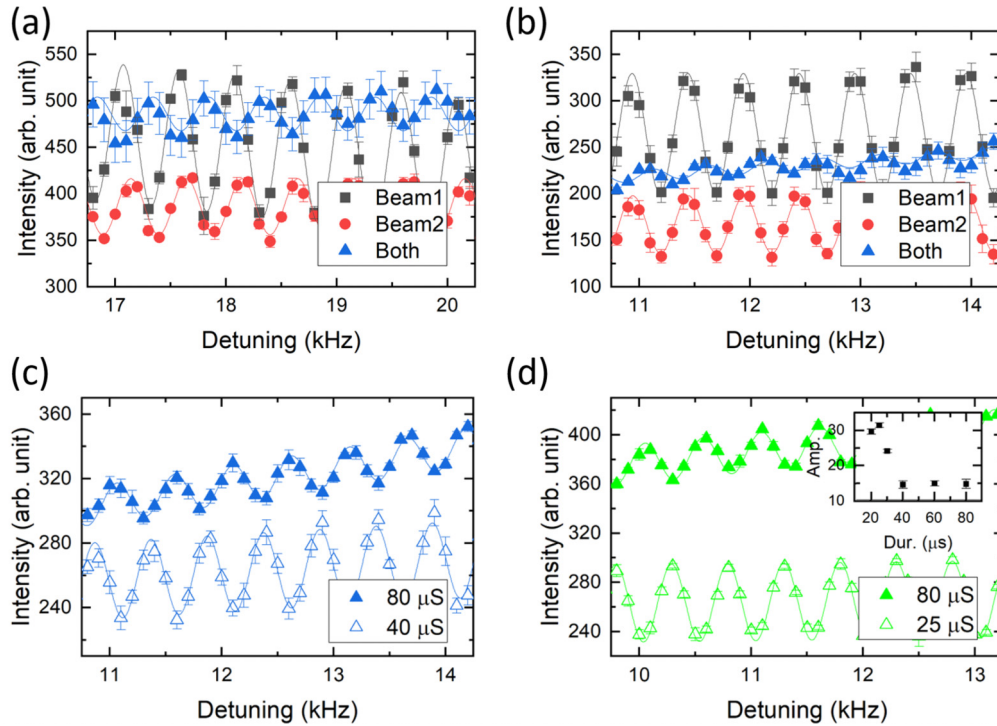
FIG. 3. Characterization of multidimensional beamsplitter properties. The plots display experimental data as dots, whereas the lines represent sine functions fitted with a linear drift, averaged over five measurements per data point. The fitted function is $A_0 \sin[(\delta - \delta_0)T] + B_0(\delta - \delta_0) + C_0$, where δ denotes the angular two-photon detuning of the Raman transitions, and T is the time separation between pulses. The detunings in all figures are $\delta/2\pi$. (a) Ramsey fringe signals obtained with two individual beams and their combination, under identical single-photon detuning for both Raman beams. (b) Ramsey fringe signals with two individual beams and their combination, but with a single-photon detuning difference of approximately 120 MHz between the two Raman beams. In both cases, the pulse duration is 80 μs. (c) Ramsey fringe signals based on two-dimensional Raman transitions, with a similar setup as in (b), albeit with different pulse durations. (d) Ramsey fringe signals based on three-dimensional Raman transitions with different pulse durations. The inset graphs the relation between the fitted amplitude A_0 and the pulse duration.

$|5S_{1/2}, F = 3\rangle \rightarrow |5P_{3/2}, F' = 4\rangle$. The population of atoms in the state $F = 2$ was detected by a charge-coupled device camera through fluorescence imaging. The time sequence of these operations is presented in Fig. 2(c).

III. RESULTS AND DISCUSSIONS

Fringes from Ramsey interferometry can be used to test the properties of the beamsplitters. We used the same configuration as that displayed in Fig. 1(a). As presented in Figs. 3(a) and 3(b), the coherence of each Raman beam-related beamsplitter was determined by the Ramsey fringes generated. The offsets in the fringes could be due to the single-photon scattering and the off-resonance of the Raman transition. The pulse duration is set to be 80 μs to achieve the highest contrasts of the fringes, which corresponds to the spectral bandwidth to be ≈10 kHz. Therefore, when we scan the two-photon detuning through a few kHz, it would be outside the center of the transition and the offset will drift.

The performance of the two-dimensional beamsplitter was demonstrated by simultaneously directing two beams to generate fringes. The difference in Figs. 3(a) and 3(b) demonstrates the indistinguishability of multidimensional photons when atoms occupy the virtual states; this is an issue associated with multidimensional multiphoton beamsplitters. In

a one-dimensional system, atoms in virtual states tend to resonate predominantly with a single electric field and then emit corresponding photons through stimulated emissions. However, in multidimensional beamsplitters, atoms in virtual states can resonate efficiently with multiple electric fields. Without precise control of the relative phases between the beams, gradual phase shifts may disturb the signals and amplify the noise, as evidenced in Fig. 3(a). To enhance signal stability and reduce noise, we introduced frequency differences in the single-photon detuning Δ across the various Raman beam directions. Due to the Fourier transform, we can estimate that the frequency difference between laser fields should be much larger than $1/\tau$, where τ is the pulse duration, to avoid interferences. Accordingly, in our setup, we set the frequency difference to 120 MHz, which helped avoid interferences. We achieved this by passing two beams through acousto-optic modulators with 200 and 80 MHz, respectively. In the original configuration displayed in Fig. 3(a), the single-photon detuning $\Delta_{x'}$ in the direction of $\hat{k}_{x'}$ is approximately 500 MHz blue-detuned from $|5S_{1/2}, F = 3\rangle \rightarrow |5P_{3/2}, F' = 4\rangle$. The single-photon detuning $\Delta_{y'}$ in the direction of $\hat{k}_{y'}$ has the same value. The result after adjusting the frequencies is shown in Fig. 3(b), here $\Delta_{x'} = 700$ MHz and $\Delta_{y'} = 580$ MHz. This modification resulted in a discernible reduction in noise compared with the initial configuration illustrated in Fig. 3(a).
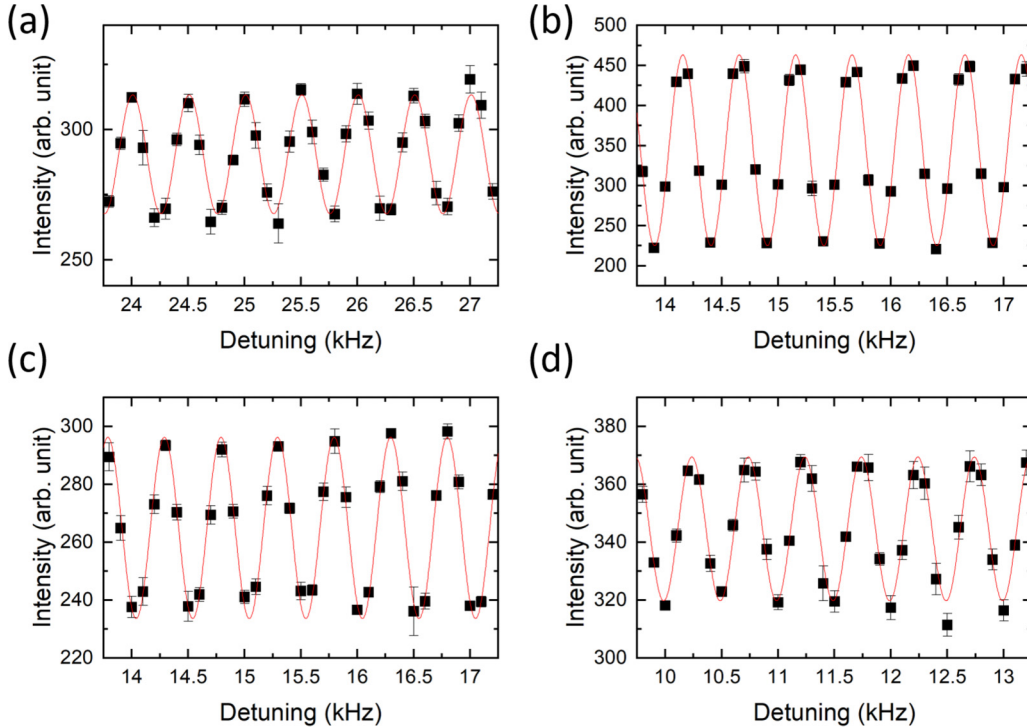
FIG. 4. Ramsey fringes under different dimensional beamsplitter configurations. Dots represent experimental data; lines are sine functions fitted to this data. Each data point is the average of five individual measurements. The fitted function is $A_0 \sin[(\delta - \delta_0)T] + C_0$. Here δ has the same definition as in Fig. 3. (a) Fringe signals with two four-photon Raman transitions in a two-dimensional plane, with configuration the same as in Fig. 1(a). The pulse duration is 40 μs. (b) Fringe signals with two two-photon Raman transitions in a two-dimensional plane, with configuration the same as in Fig. 1(b). The pulse duration is 20 μs. (c) Fringe signals with two four-photon Raman transitions and one two-photon Raman transition in a three-dimensional space, with configuration the same as in Fig. 1(c). The pulse duration is 25 μs. (d) Fringe signals with three two-photon Raman transitions in a three-dimensional space, with configuration the same as in Fig. 1(d). The pulse duration is 20 μs.

The fringes in Fig. 3(b) can be further improved by reducing the pulse duration, as demonstrated in Fig. 3(c). For better demonstration, we employed the same frequency scanning range as that used for the results in Fig. 3(b). In addition to the wider Fourier transform of the pulses compensating the ac Stark shift better, the superposition of states in the multidimensional beamsplitters played a role in the improvement. Activating multiple Raman beams simultaneously does not guarantee that atoms achieve a superposition of multiple virtual excited states during the transition. To further verify the superposition, we considered the amplitudes in scenarios where potential pathways in a beamsplitter could lead to similar final states in the Ramsey interferometer. These amplitudes should sum up coherently rather than accumulate individually. When atoms are initially in the $|0\rangle$ state, after a perfect $\pi/2$ beamsplitter the quantum state should being transferred as $|0\rangle \rightarrow (|0\rangle + |1\rangle)/\sqrt{2}$. When two beamsplitters are happening at the same time, then we can write $|0\rangle \rightarrow a|0\rangle + b|1\rangle + c|1'\rangle$, where a, b, and c are complex numbers and $|a|^2 + |b|^2 + |c|^2 = 1$. In general $|1\rangle$ and $|1'\rangle$ represent atoms with the same internal state but different external states since atoms absorb momentum from photons in different directions. However, for copropagating beams the momentum difference is small and we can assume $|1\rangle \approx |1'\rangle$ and the relation becomes $|a|^2 + |b + c|^2 = 1$. For optimal contrast, we should have $|a| = 1/\sqrt{2}$ and $|b| = |c| = 1/(2\sqrt{2})$. This

implies that the reduction of the pulse duration in the Ramsey interferometer should enhance the overall contrast when compared with the use of a single Raman beam. The results are demonstrated in Fig. 3(c), with pulse duration set to be $80/2 = 40$ μs.

A further example can be demonstrated in the three-dimensional case, where the pulse duration should be even shorter. Figure 3(d) presents a comparison of the results obtained using the original 80-μs pulse duration with those obtained using the reduced duration, $80/3 \approx 26.6 \approx 25$ μs. Here we are using the configuration demonstrated in Fig. 1(c), and the single-photon detuning $\Delta_{z'}$ in the direction of $\hat{k}_{z'}$ is about 500 MHz blue-detuned from $|5S_{1/2}, F = 3\rangle \rightarrow |5P_{3/2}, F' = 4\rangle$. As illustrated by the inset of Fig. 3(d), the fringe contrast peaked at approximately 25 μs, aligning with our predictions. Owing to the discrepancy in power distribution among all three beams, the contrast did not decrease to zero for longer pulses approaching the π-π pulse sequence in the Ramsey interferometry.

Multiple methods exist for driving multidimensional beamsplitters. As demonstrated in the Introduction, there are at least two configurations for two-dimensional and three-dimensional cases, respectively. The related fringes are shown in Fig. 4. Here we use a different approach compared to Fig. 3. We keep the power around the same level for different configurations in two-dimensional and three-dimensional
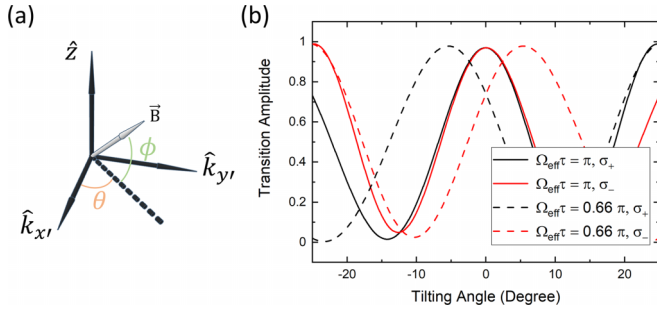
FIG. 5. Properties related to the alignment of the quantization axes. (a) Scheme for demonstration of the tilting magnetic field as the external quantization axis. (b) Calculation of the four-photon transition amplitude under different tilting angles, here indicated as $\pi/2 - \phi$. Solid lines and dashed lines represent different intensities of the laser beams, which indicate different Ω_{eff}. Different polarizations are represented by different colors.

cases, respectively. The power for the two-dimensional cases is about 600 µW and for the three-dimensional cases is about 700 µW. After tuning the intensity distribution to achieve similar Rabi oscillation performances in different directions, we adjust the pulse duration to improve the contrast signals. As demonstrated in Figs. 4(a) and 4(b), the contrast in the two-dimensional case with two-photon Raman transitions is much better than the four-photon one. However, for the three-dimensional case, as shown in Figs. 4(c) and 4(d), there are not too many differences between them. This is because, in the three-dimensional beamsplitter, the effectiveness of two-photon Raman transitions diminished when the quantization axis diverged from being parallel to the beam direction. A combination of two four-photon and one two-photon Raman transitions could result in more efficient optical power utilization, despite the usual higher power requirement of four-photon transitions.

We demonstrated the performance of the developed multidimensional beamsplitters with various configurations. The findings reveal that the primary differences among these configurations were related to the orientation of the magnetic field, which serves as the quantization axis. We will therefore discuss the situation where the axis is away from the assigned direction. The parameters we used to consider the alignment are represented in Fig. 5(a). As the two-photon Raman transition can be used to achieve parallel alignment between the beams and the external magnetic field, four-photon Raman transitions can be used to achieve perpendicular alignment between the beams and the magnetic field. Combining two-photon and four-photon Raman transitions, we can also ensure orthogonal alignments between beams. On the basis of relevant studies on multiphoton Raman transitions under different quantization axes [33], we determined that equal signal intensities for different polarizations, namely σ^+ and σ^-, could be attained when the beam is perpendicular to the quantization axis, as displayed in Fig. 5(b). Therefore, by comparing signals across polarizations, we could ensure the beams are perpendicular to the external magnetic field. This method streamlines the alignment of the quantization axis in multidimensional beamsplitters involving four-photon Raman transitions, particularly

when the axis aligns with the beams, as illustrated in Figs. 1(a) and 1(c).

The deviation of the axis will happen more easily for the two-photon Raman transitions-only configurations. In practice, the alignment of two-photon Raman transitions in one dimension is optimized by maximizing signal strength using reduced optical power. This method is not feasible for two-dimensional or three-dimensional beamsplitters relying solely on two-photon Raman transitions, as displayed in Figs. 1(b) and 1(d), since the assigned quantization axis will not make maximum signals. It becomes ambiguous if the increased signals come from the misalignment or from hitting more atoms. Therefore, we will focus our discussion on the deviation with two-photon Raman transitions-only cases.

The misalignment of the quantization axis in a two-photon Raman process would make not only a loss of contrast but also statistical and systematic errors. For demonstration, we are considering the proposed square two-dimensional Mach-Zehnder interferometry [19], as displayed in Fig. 6(a). In a one-dimensional Mach-Zehnder interferometry case, the relative phase from atom-light interaction in a beamsplitter is often overlooked, since the Mach-Zehnder configuration will, in general, cancel out the phase contributions from atom-light interaction of the same kind of beamsplitter. In a multidimensional case, however, things are not the same. When there is more than one kind of beamsplitter, as comes from asymmetric quantization axes between Raman transitions, the relative phase may not be totally canceled out. This situation is similar to that observed in Bragg diffractions-based Ramsey-Bordé atom interferometry [34], wherein the phase contribution from atom-light interactions plays a crucial role in the systematic errors.

Based on the model established in our previous study [33], we can calculate the amplitude and relative phase when two Raman pulses drive the transition at the same time as a two-dimensional beamsplitter with different external magnetic fields as quantization axes. Calculation results obtained for $\pi/2$ and π beamsplitters are shown in Figs. [6(b)–6(e)]. For a $\pi/2$ beamsplitter, atoms are initially set in $|F = 3, 0, 0, 0\rangle$, where the states are labeled by their internal state and the momentum transfer along each direction of the Raman beams. For a π beamsplitter, we assume atoms are following path A in Fig. 6(a) and are initially in the $|F = 2, \hbar\Delta k_{x'}, 0, 0\rangle$ state.

From calculations in Figs. [6(b)–6(e)], we could infer that in a square two-dimensional Mach-Zehnder interferometer, atoms could obtain different relative phases due to their thermal velocities, which contribute to statistical errors. If we assume the ^{85}Rb atoms are cooling down to the recoil temperature range in all directions, whose corresponding Doppler shift will be about 3.86 kHz in the D_2 line, then the phase shifts that form the statistical errors will be estimated about ≈ 1 rad per atom.

Besides statistical errors, different quantization axes will change the ratio between π, σ^+, and σ^- Zeeman transitions in atoms and will change the relative contributions to the ac Stark shifts. When single-photon detuning Δ is not infinite, the resonance deviation from ac Stark shift will bring out extra phase shifts. These phase shifts are constant and become particularly pronounced when the measured rotation and acceleration are small. We could consider the case in
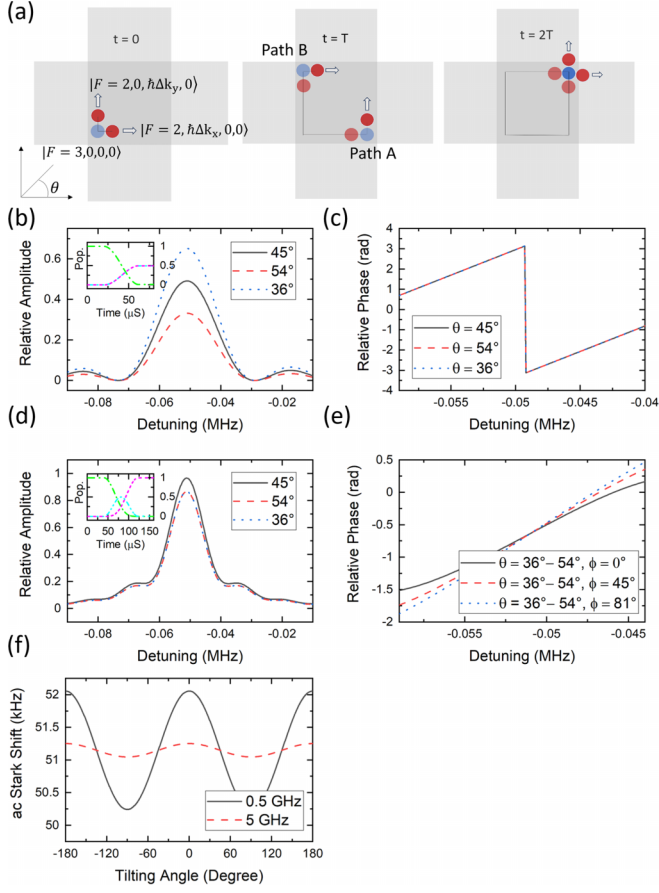
FIG. 6. Calculated properties related to two-dimensional Raman transitions under different quantization axes. (a) Top view schematic of a sequence constituting a two-dimensional Mach-Zehnder interferometer using atom-optical pulses, assuming pulse duration τ is much smaller compared to T. Gray rectangular areas represent the Raman beams. (b) Calculated $|F = 2, \hbar\Delta k_{x'}, 0, 0\rangle$ amplitudes after the two-dimensional $\pi/2$ beamsplitter. Here each Raman pulse is set to be 40 μs and the intensity is set to achieve an overall $\pi/2$ transition for each output with $\theta = 45°$ and $\phi = 0$. The inset demonstrates the population transfer of the three states of the atoms during the beamsplitter process. (c) Calculated relative phases between $|F = 3, 0, 0, 0\rangle$ before the pulse and $|F = 2, \hbar\Delta k_{x'}, 0, 0\rangle$ after the pulse under different θ. The conditions for the Raman pulses are the same as in (b). Calculation results with different ϕ are similar. (d) Calculated $|F = 2, 0, \hbar\Delta k_{y'}, 0\rangle$ amplitudes after the two-dimensional π beamsplitter based on a pair of two-photon Raman transitions. Here each Raman pulse is set to be 80 μs and the intensity is set to achieve an overall π transition with $\theta = 45°$ and $\phi = 0$. The inset demonstrates similar population transfers of the atoms as in (b). (e) Calculated relative phases between $|F = 2, \hbar\Delta k_{x'}, 0, 0\rangle$ before the pulse and $|F = 2, 0, \hbar\Delta k_{y'}, 0\rangle$ after the pulse under different θ and ϕ. The conditions for the Raman pulses are the same as in (d). (f) Calculated ac Stark shifts relative to different tilting angles of quantization axes under different single-photon detunings.

the proposed multidimensional atom interferometry [19] as an example, and assuming using ^{85}Rb. Given interrogation time T as 30 ms, wavelength as 780 nm, and the earth rotation rate

as 7.3×10^{-5} rad/s, we can estimate that the phase difference related to the rotation $\Delta\Phi$ will be about 25.3 mrad per shot. Given 500 MHz blue-detuned away from $|5S_{1/2}, F = 3\rangle \rightarrow |5P_{3/2}, F' = 4\rangle$ in the ^{85}Rb case, the ac Stark shift calculation is shown in Fig. 6(f). Based on the shift, we can estimate the extra systematic error from the misaligned quantization axis. The relative uncertainty from the state-of-the-art inertial sensor [7] is demonstrated as $0.05/5.5 \approx 0.91\%$, which will lead 0.23 mrad here. Therefore, the alignment of the quantization axis could be better to be within approximately 10^{-2}-deg range. From the estimations, we can see in some cases the alignment would be an issue of concern.

In addition to the approach of making appropriate alignments, another approach entails measuring the related frequency at different values of T to account for the constant phase shift [34]. Because the constant phase offset from atom-light interactions contributes to the measured frequency, which is inversely proportional to T, the frequency has a linear relation with $1/T$. By fitting the frequencies measured at different T, one can effectively eliminate the extra constant phase shift. This approach will encounter the power distribution issue in the original multidimensional atom interferometry design, in which there will be one beam in each direction to drive multiple beamsplitters at different locations. Varying power distributions in the Raman beams leads to different ac Stark shifts, causing an atom interferometer to retain different phases at different time intervals. A potential solution is to expand the beams, necessitating increased optical power. Similarly, we can increase Δ to suppress the effect of ac Stark shift, as also demonstrated in Fig. 6(f). It also implies higher optical power requirements.

IV. CONCLUSION

In summary, we realize multidimensional matter-wave beamsplitters, which pave a way for future applications in multidimensional atom interferometers or even higher-dimensional quantum information applications. Our experimental results validate several predicted phenomena in multidimensional beamsplitters, including parasitic resonances and alterations in the efficient pulse durations of Ramsey fringes. In addition to the conventional design of using two-photon Raman transitions, we incorporated recently discovered four-photon Raman transitions to construct beamsplitters and conducted comparative analyses. The tradeoff between the potential errors and power requirement when choosing the proper direction of the external magnetic fields is discussed and could be evaluated in future multidimensional applications using Raman transitions.

ACKNOWLEDGMENTS

[1] D. S. Weiss, B. C. Young, and S. Chu, Phys. Rev. Lett. **70**, 2706 (1993).

[2] A. Peters, K. Y. Chung, and S. Chu, Nature (London) **400**, 849 (1999).

[3] T. Gustavson, A. Landragin, and M. Kasevich, Classical Quantum Gravity **17**, 2385 (2000).

[4] A. Wicht, J. M. Hensley, E. Sarajlic, and S. Chu, Phys. Scr. **2002**, 82 (2002).

[5] R. Bouchendira, P. Cladé, S. Guellati-Khélifa, F. Nez, and F. Biraben, Phys. Rev. Lett. **106**, 080801 (2011).

[6] F. Sorrentino, A. Bertoldi, Q. Bodart, L. Cacciapuoti, M. De Angelis, Y.-H. Lien, M. Prevedelli, G. Rosi, and G. Tino, Appl. Phys. Lett. **101**, 114106 (2012).

[7] B. Canuel, F. Leduc, D. Holleville, A. Gauguet, J. Fils, A. Virdis, A. Clairon, N. Dimarcq, C. J. Bordé, A. Landragin *et al.*, Phys. Rev. Lett. **97**, 010402 (2006).

[8] P. Hamilton, M. Jaffe, P. Haslinger, Q. Simmons, H. Müller, and J. Khoury, Science **349**, 849 (2015).

[9] T. H. Kim, S. H. Yim, K. M. Shim, and S. Lee, Phys. Rev. A **95**, 033632 (2017).

[10] X. Wu, F. Zi, J. Dudley, R. J. Bilotta, P. Canoza, and H. Müller, Optica **4**, 1545 (2017).

[11] R. H. Parker, C. Yu, W. Zhong, B. Estey, and H. Müller, Science **360**, 191 (2018).

[12] Y. Bidel, N. Zahzam, C. Blanchard, A. Bonnin, M. Cadoret, A. Bresson, D. Rouxel, and M. Lequentrec-Lalancette, Nat. Commun. **9**, 627 (2018).

[13] G. M. Tino, Quantum Sci. Technol. **6**, 024014 (2021).

[14] T. L. Gustavson, P. Bouyer, and M. A. Kasevich, Phys. Rev. Lett. **78**, 2046 (1997).

[15] M. J. Snadden, J. M. McGuirk, P. Bouyer, K. G. Haritos, and M. A Kasevich, Phys. Rev. Lett. **81**, 971 (1998).

[16] J. K. Stockton, K. Takase, and M. A. Kasevich, Phys. Rev. Lett. **107**, 133001 (2011).

[17] I. Dutta, D. Savoie, B. Fang, B. Venon, C. Garrido Alzar, R. Geiger, and A. Landragin, Phys. Rev. Lett. **116**, 183003 (2016).

[18] K. S. Hardman, P. J. Everitt, G. D. McDonald, P. Manju, P. B. Wigley, M. A. Sooriyabandara, C. C. N. Kuhn, J. E. Debs, J. D. Close, and N. P. Robins, Phys. Rev. Lett. **117**, 138501 (2016).

[19] B. Barrett, P. Cheiney, B. Battelier, F. Napolitano, and P. Bouyer, Phys. Rev. Lett. **122**, 043604 (2019).

[20] A. Schreiber, A. Gábris, P. P. Rohde, K. Laiho, M. Štefaňák, V. Potoček, C. Hamilton, I. Jex, and C. Silberhorn, Science **336**, 55 (2012).

[21] H. Tang, X.-F. Lin, Z. Feng, J.-Y. Chen, J. Gao, K. Sun, C.-Y. Wang, P.-C. Lai, X.-Y. Xu, Y. Wang *et al.*, Sci. Adv. **4**, eaat3174 (2018).

[22] A. W. Young, W. J. Eckner, N. Schine, A. M. Childs, and A. M. Kaufman, Science **377**, 885 (2022).

[23] M. Mohseni, P. Rebentrost, S. Lloyd, and A. Aspuru-Guzik, J. Chem. Phys. **129**, 174106 (2008).

[24] T. Kitagawa, M. S. Rudner, E. Berg, and E. Demler, Phys. Rev. A **82**, 033429 (2010).

[25] A. Ambainis, Int. J. Quantum. Inform. **01**, 507 (2003).

[26] A. M. Childs and J. Goldstone, Phys. Rev. A **70**, 022314 (2004).

[27] A. Tulsi, Phys. Rev. A **78**, 012310 (2008).

[28] H. Müller, S.-W. Chiow, and S. Chu, Phys. Rev. A **77**, 023609 (2008).

[29] E. Giese, A. Roura, G. Tackmann, E. M. Rasel, and W. P. Schleich, Phys. Rev. A **88**, 053608 (2013).

[30] P. Cladé, Riv. Nuovo Cim. **38**, 173 (2015).

[31] Z. Pagel, W. Zhong, R. H. Parker, C. T. Olund, N. Y. Yao, and H. Müller, Phys. Rev. A **102**, 053312 (2020).

[32] R. B. Li, P. Wang, H. Yan, J. Wang, and M. S. Zhan, Phys. Rev. A **77**, 033425 (2008).

[33] J.-W. Chang, Y.-C. Huang, Z.-W. Xu, Y.-H. Kan, H.-H. Huang, J.-Z. Huang, K.-J. Fu, X.-D. Liu, and P.-C. Kuan, Phys. Rev. A **108**, 013308 (2023).

[34] B. Estey, C. Yu, H. Müller, P.-C. Kuan, and S.-Y. Lan, Phys. Rev. Lett. **115**, 083002 (2015).